

The mean solar butterfly diagram and poloidal field generation rate at the surface of the Sun

S. Cloutier¹, R. H. Cameron¹, and L. Gizon^{1,2}

¹ Max-Planck-Institut für Sonnensystemforschung, Justus-von-Liebig-Weg 3, D-37077 Göttingen, Germany
e-mail: cloutier@mps.mpg.de

² Institut für Astrophysik und Geophysik, Georg-August-Universität Göttingen, D-37077 Göttingen, Germany

May 28, 2024

ABSTRACT

Context. The difference between individual solar cycles in the magnetic butterfly diagram can mostly be ascribed to the stochasticity of the emergence process.

Aims. We aim to obtain the expectation value of the butterfly diagram from observations of four cycles. This allows us to further determine the generation rate of the surface radial magnetic field.

Methods. We use data from Wilcox Solar Observatory to generate time-latitude diagrams spanning cycles 21 to 24 of the surface radial and toroidal magnetic fields, symmetrize them across the equator and cycle-average them. From the mean butterfly diagram and surface toroidal field we then infer the mean poloidal field generation rate at the surface of the Sun.

Results. The averaging procedure removes realization noise from individual cycles. The amount of emerging flux required to account for the evolution of the surface radial field is found to match that provided by the observed surface toroidal field and Joy's law.

Conclusions. Cycle-averaging butterfly diagrams removes realization noise and artefacts due to imperfect scale separation, and corresponds to an ensemble average that can be interpreted in the mean-field framework. The result can then be directly compared to $\alpha\Omega$ -type dynamo models. The Babcock-Leighton α -effect is consistent with observations, a result that can be appreciated only if the observational data is averaged in some way.

Key words. Sun: magnetic fields – Sun: activity

1. Introduction

The solar cycle lasts on average approximately 11 years and is believed to be driven by a hydromagnetic dynamo seated in the convection zone of the Sun (Charbonneau 2020). The dynamo loop consists of two parts; one where toroidal field is generated from the poloidal field, and another where poloidal field of opposite sign is generated from the new toroidal field. It takes another solar cycle, or half of the magnetic cycle, to revert to the original polarity. The first part is relatively well understood and takes place through the so-called Ω -effect, whereby poloidal field is wound up in the azimuthal direction by the differential rotation, which is observationally well constrained by helioseismology (eg. Schou et al. 1998). The second part, on the other hand, involves the unobservable subsurface toroidal field and two possible mechanisms; the turbulent α -effect (Parker 1955a; Steenbeck et al. 1966) and the Babcock-Leighton (BL) mechanism (Babcock 1961; Leighton 1964, 1969). Since the latter can also be put in a functional form identical to the former, it is sometimes called the BL α -effect.

The mean field of mean-field electrodynamics is defined in terms of an average that can either be spatial, temporal or ensemble. In the case of the Sun, the azimuthal average is a natural choice. In fact, the butterfly diagram is constructed by longitudinally averaging line-of-sight synoptic magnetograms. The symmetric component (with respect with the solar meridian) is then extracted, from which the radial field is obtained by assuming it is the only component of the poloidal field at the surface. Finally, the butterfly diagram is obtained by stacking the result in time.

In principle, butterfly diagrams are thus of mean-field nature and can be directly compared to models.

A caveat, however, is that scale separation is likely to be poor in the Sun as supergranulation reaches down to about 5% of the solar radius, which is non-negligible with respect to the size of the convection zone and the scales of the differential rotation and meridional flow. The picture is much worse if we consider the scale of active regions, which is on the order of 100 Mm, about half the depth of the convection zone. Consequently the observed butterfly diagram can't be directly compared to simple mean-field models aimed at reproducing the most fundamental features of the solar cycle. A way to circumvent this is by considering different solar cycles as different realizations of the dynamo, and ensemble average them (note that this is not a true ensemble average in the mean-field sense, cf. Hoyng 2003, but is aimed at reproducing the azimuthal average used in models with reduced realization noise). In other words, average different cycles together to remove realization noise (fluctuating dynamo parameters) and the effects of imperfect scale separation.

The way cycles are to be averaged together requires careful consideration. It has been shown that defining cycles in terms of activity minimum or maximum is not ideal (Waldmeier 1955; Hathaway 2011). Nevertheless, observations show that all cycles present the same equatorward pattern of sunspot migration, regardless of strength (Waldmeier 1939; Hathaway 2011). When cycles are defined according to the time the centroid of sunspot area reach a certain latitude, they all behave the same way; the location of this centroid migrates equatorward according to the same standard law (Hathaway 2011). For this reason, we define

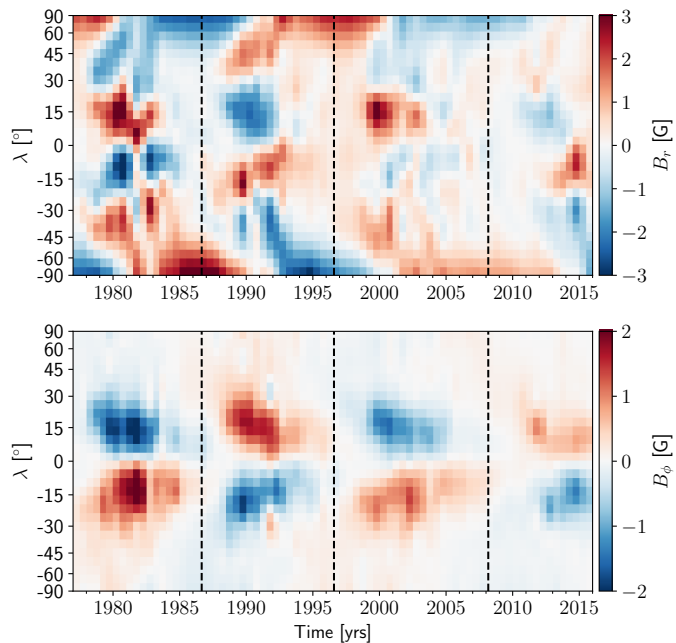


Fig. 1. Time-latitude diagrams of the surface radial field B_r (top) and of the surface toroidal field B_ϕ (bottom). The vertical dotted lines indicate the cycle start times as given by the times where the central latitude of the sunspot belts reach 19° minus 4 years.

the reference times as 4 years before the times when the centroid of sunspot area reach 19° (Cameron & Schüssler 2023). The individual cycles are then averaged together in phase. To carry out this cycle-averaging we use butterfly diagrams produced from synoptic magnetograms obtained by the Wilcox Solar Observatory (WSO). We further symmetrize the data across the equator so that we have, in effect, an average consisting of 8 cycles.

In addition to the surface radial field, another important quantity we can infer from longitudinally-averaged line-of-sight magnetograms is the toroidal field emerging at the surface, the antisymmetric component (with respect to the solar meridian), from which we can construct a time-latitude diagram (from WSO data, Cameron et al. 2018). Having both mean time-latitude diagrams of the surface radial and toroidal fields at our disposal, we can test the validity of the simple $\alpha\Omega$ dynamo models, as well as possibly constrain the functional form of the source term. To do this, we calculate independently from both quantities an intermediate one: the surface radial field generation rate – the radial source term. This quantity can be inferred from the radial field butterfly diagram using the surface flux transport (SFT) model (Leighton 1964; DeVore et al. 1984; Sheeley et al. 1985), and independently from the surface toroidal field butterfly diagram using Joy’s law. Both diagrams are then compared to determine if they are consistent with each other.

2. The observed mean butterfly diagram

The WSO data we use is presented in Figure 1. Also shown are the reference start times of the individual cycles, defined by the time when the central latitude of the activity belts reach 19° minus 4 years (Cameron & Schüssler 2023).

We have 4 cycles of data for 2 hemispheres, so that we have in effect 8 cycles to average together. We perform the cycle-averaging as follows: we first symmetrize the data across the equator, then for each cycle shift the butterfly diagram starting

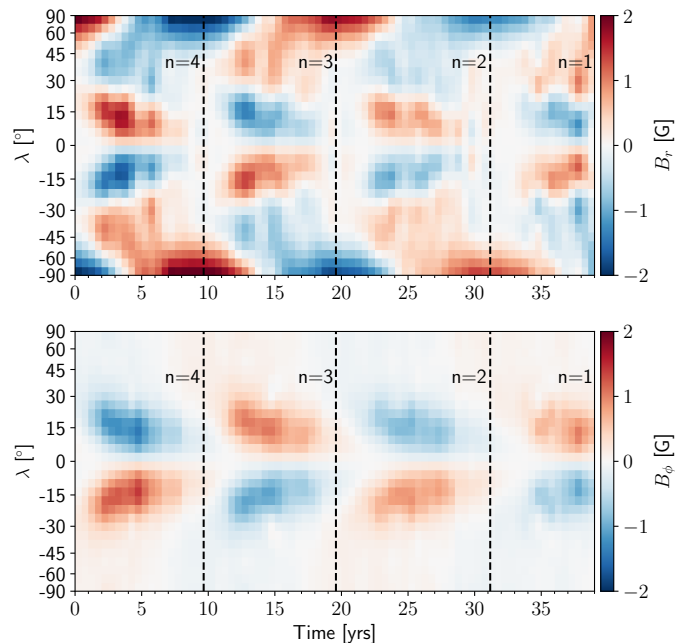


Fig. 2. Time-latitude diagrams of the cycle-averaged surface radial field B_r (top) and of the surface toroidal field B_ϕ (bottom). The vertical dotted lines indicate the cycle start times as given by the times where the central latitude of the sunspot belts reach 19° minus 4 years.

from that cycle backwards to the reference time of cycle 21, and average. The result of this procedure is shown in Figure 2. It consists of 4 averages of the solar cycles obtained by a decreasing amount of cycles.

One can immediately see that the cycle-averaging produces butterfly wings that are much better defined. We have clear butterfly wings of one polarity, that of the leading sunspots, and poleward migrating fields of the opposite polarity, that of the trailing sunspots. The latter feature is also known as the "rush to the poles" (Ananthakrishnan 1954). Even with only 8 realizations, the trailing polarity field is essentially removed from the butterfly wings. The rush to the poles is also increasingly filled with fields of trailing polarity and devoid of fields of leading polarity. We thus see a "separation of polarities" happening. The butterfly wings are much more clearly delineated and seem narrower with a width slightly under 30° , rather than one of $\approx 35^\circ$. Lastly, the rapid increase of sunspot number during the rising phase, and its slow decrease during the declining phase is much more apparent.

It is clear, however, that 4 solar cycles is not nearly enough to carry out a proper ensemble average. It is nonetheless reasonable, from these results, to assume that the addition of more cycles would further the observed trend. Most of the small-scale features will be washed out and the mean observed butterfly diagram will look very similar to those calculated from mean-field dynamo models; smooth butterfly wings of the leading spot polarity, and rush to the poles and polar fields of trailing spot polarity.

Note the change of the scaling from Figure 1 to 2. The largest fields inside the butterfly wings are brought down from 3 G to 2 G. Higher-resolution butterfly diagrams (eg. Norton et al. 2023) have fields the order of 10 G; in WSO data part of the averaging has already been done by the instrument’s limited resolution. This is more evidence that one needs to be careful when comparing simulation results from mean-field models to observations.

3. Inferring the radial field generation rate

The radial field generation rate, or the radial source term, can be inferred both through the butterfly diagram and the time-latitude diagram of the surface toroidal field, by making use of models of surface flux transport (SFT) and emergence (BL mechanism).

3.1. Surface flux transport model

The SFT model describes the passive advective and diffusive transport of the surface radial field by the following equation (Yeates et al. 2023):

$$\begin{aligned} \frac{\partial B_r}{\partial t} = & -\omega(\lambda) \frac{\partial B_r}{\partial \phi} - \frac{1}{R_\odot \cos \lambda} \frac{\partial}{\partial \lambda} (\cos \lambda v(\lambda) B_r) \\ & + \frac{\eta}{R_\odot^2} \left[\frac{1}{\cos \lambda} \frac{\partial}{\partial \lambda} \left(\cos \lambda \frac{\partial B_r}{\partial \lambda} \right) + \frac{1}{\cos^2 \lambda} \frac{\partial^2 B_r}{\partial \phi^2} \right] + S_r(\lambda, \phi, t), \end{aligned} \quad (1)$$

where B_r , $\omega(\lambda)$, $v(\lambda)$, η , and $S_r(\lambda, \phi, t)$ are respectively the surface radial field, angular velocity, meridional flow, diffusivity, and radial source term, λ is the latitude and ϕ the longitude. Since the magnetic butterfly diagram provides us the longitudinally-averaged surface radial field $B_r(\lambda, t)$, the only unknown is the surface radial source term

$$\begin{aligned} S_r(\lambda, t) = & \frac{\partial B_r}{\partial t} + \frac{1}{R_\odot} \frac{\partial}{\partial \sin \lambda} (\cos \lambda v(\lambda) B_r) \\ & - \frac{\eta}{R_\odot^2} \frac{\partial}{\partial \sin \lambda} \left(\cos^2 \lambda \frac{\partial B_r}{\partial \sin \lambda} \right). \end{aligned} \quad (2)$$

We use a value of turbulent diffusivity of $\eta = 350 \text{ km}^2/\text{s}$, which is consistent with estimates from observations (eg. Komm et al. 1995), the SFT model of Lemerle et al. (2015) and MLT (eg. Muñoz-Jaramillo et al. 2011). As for the surface meridional flow profile, we use the anti-symmetrized time-dependent profiles obtained from the helioseismic inversions of Gizon et al. (2020).

3.2. Emergence model

There is strong evidence (see eg. Dasi-Espuig et al. 2010; Kitchatinov & Olemsky 2011; Cameron & Schüssler 2015) that suggests the BL mechanism is the main poloidal field generation mechanism of the solar dynamo. The first part of this mechanism is the emergence through the photosphere of tilted toroidal flux tubes. The corresponding generation of (radial) poloidal field from the emerging toroidal field can be derived as follows.

We begin with the solenoidal condition $\nabla \cdot \mathbf{B} = 0$ for an axisymmetric field \mathbf{B} ,

$$\frac{\partial(r^2 B_r)}{\partial r} + \frac{r}{\sin \theta} \frac{\partial(B_\theta \sin \theta)}{\partial \theta} = 0. \quad (3)$$

Next, we integrate in r from the surface to infinity and take the time derivative to obtain

$$\frac{\partial B_r|_{R_\odot}}{\partial t} = -\frac{1}{R_\odot^2} \int_{R_\odot}^{\infty} \frac{r}{\sin \theta} \frac{\partial^2(B_\theta \sin \theta)}{\partial \theta^2} dr. \quad (4)$$

Joy's law implies that as flux is emerging through the photosphere $B_\theta = B_\phi \tan \delta$, where δ is the tilt angle of the resulting bipolar magnetic region. The rate at which the flux of B_ϕ is carried through the surface per radian in θ is

$$\frac{\partial}{\partial t} \int_{R_\odot}^{\infty} B_\theta r dr = -R_\odot v_e B_\phi|_{R_\odot}, \quad (5)$$

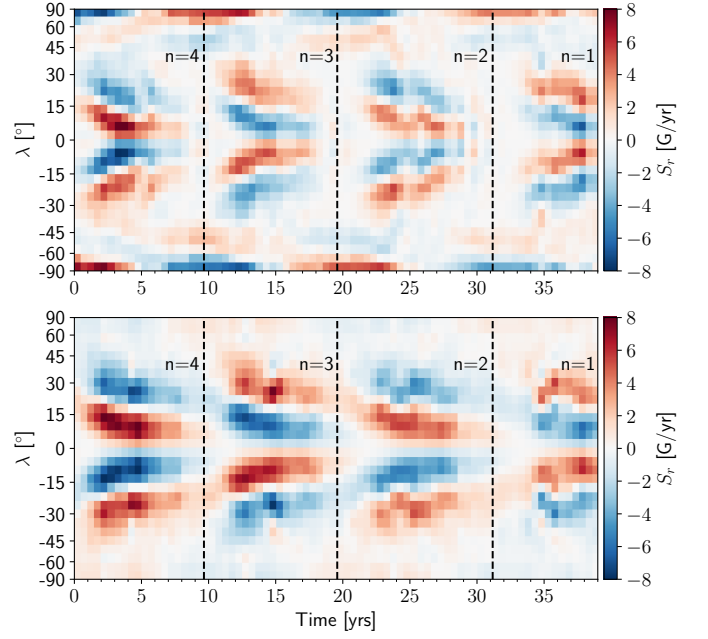


Fig. 3. *Left panel:* time-latitude diagrams of the surface radial source term S_r inferred from the high-res (top) and low-res (middle) data by use of the SFT model, and from the low-res surface toroidal field (bottom). The vertical dotted lines indicate the cycle start times as given by the times where the central latitude of the sunspot belts reach 19° minus 4 years.

where v_e is the radial velocity of the emerging field. Then

$$\begin{aligned} \frac{\partial}{\partial t} \int_{R_\odot}^{\infty} B_\theta r dr &= \tan \delta \frac{\partial}{\partial t} \int_{R_\odot}^{\infty} B_\phi r dr, \\ &= -\tan \delta R_\odot v_e B_\phi. \end{aligned} \quad (6)$$

This yields, for the surface radial field generation rate,

$$\frac{\partial B_r|_{R_\odot}}{\partial t} = \frac{1}{R_\odot \sin \theta} \frac{\partial}{\partial \theta} (\sin \theta \tan \delta v_e B_\phi), \quad (7)$$

or, with $\cos \delta \sim 1$,

$$S_r(\lambda, t) = -\frac{1}{R_\odot} \frac{\partial}{\partial \sin \lambda} (\cos \lambda \sin \delta v_e B_\phi). \quad (8)$$

We use the form of Joy's law as given by Leighton (1969), $\sin \delta = 0.5 \sin \lambda$. As for the emergence velocity, we consider three different prescriptions. The first is the constant velocity of $v_e \simeq 200 \text{ m/s}$ inferred by Centeno (2012). We also consider the cases where the emergence velocity v_e is proportional to the toroidal field B_ϕ (Parker 1955b) or to its square B_ϕ^2 (Unno & Ribes 1976). We thus write the emergence velocity as

$$v_e = \left[\frac{|B_\phi|}{\max(B_\phi)} \right]^m v_0, \quad (9)$$

where $v_0 = 200 \text{ m/s}$ and $m \in \{0, 1, 2\}$.

4. The observed mean radial field generation rate

The mean surface radial field generation rates S_r , as inferred from the surface radial and toroidal fields, are shown in Figure 3. We clearly see one "mean BMR" inside the activity belts. Remarkably, both methods used to infer the radial field generation

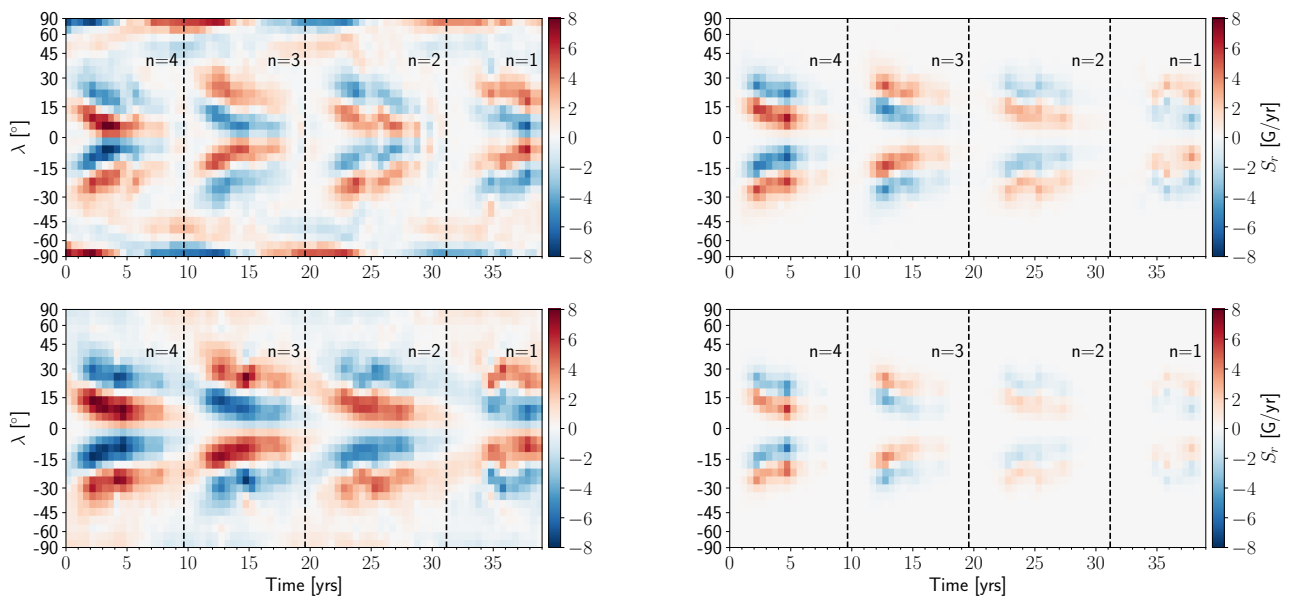


Fig. 4. Time-latitude diagrams of the surface source term as obtained from the SFT model (upper left) and emergence model with different emergence velocity prescriptions; constant velocity (lower left), linear (upper right) and quadratic (lower right) toroidal field dependence on the emergence velocity.

rate give results in good qualitative agreement, including both the shape of the mean BMRs and their amplitudes. There are, however, three main noticeable discrepancies. Firstly, the SFT model gives us important radial field generation at the poles, of the opposite polarity to that of the polar fields. This could be explained by underestimated polar field strengths from the observations (Linker et al. 2017), possibly in combination with a weakened meridional flow amplitude at latitudes above 60° (Mahajan et al. 2021). Secondly, there are sorts of weak amplitude "bridges" at cycle minimum between the poleward polarity of one cycle and the equatorward polarity of the next (showcasing the magnetic cycle and activity overlap between cycles). This overlap is only visible in the S_r obtained through the surface toroidal field and Joy's law. Thirdly, the source term derived from the surface toroidal field and Joy's law are slightly wider and are shifted slightly polewards compared to those obtained from the surface radial field.

Lastly, we consider emergence velocities of the toroidal field depending linearly and quadratically on the toroidal field strength. The result is presented in Figure 4. We see that increasing this dependence makes the mean BMR restricted to increasingly lower latitudes. Furthermore, in both the linear and quadratic cases, the aforementioned "bridges" between sunspot cycles seen in the constant velocity case disappear. Since the bridges are lacking in the source term necessary to explain the evolution of the surface radial field, this suggests that either Joy's law or the emergence velocity of low flux regions might differ from that of active regions.

5. Conclusion

In this paper we have shown that one must be careful when comparing butterfly diagrams produced by simple mean-field models with observed ones. Because of imperfect scale separation, the use of the azimuthal average does not result in an observed butterfly diagram that can be understood in the mean-field sense. The observed butterfly diagram must for this be cycle-averaged,

a procedure made possible by the universality of the equatorward sunspot belt migration.

By making use of the average toroidal field butterfly diagram and Joy's law, we found the α -effect-like BL source term is qualitatively consistent in shape and amplitude with the source term as inferred from the SFT model and the radial field butterfly diagram. This consistency is further increased when we assume the toroidal field emergence velocity to be dependent on the toroidal field strength itself.

Acknowledgements. This work was carried out when SC was a member of the International Max Planck Research School for Solar System Science at the University of Göttingen. The authors acknowledge partial support from ERC Synergy grant WHOLE SUN 810218.

References

- Ananthakrishnan, R. 1954, Proceedings of the Indian Academy of Sciences-Section A, 40, 72
- Babcock, H. W. 1961, ApJ, 133, 572
- Cameron, R. & Schüssler, M. 2015, Science, 347, 1333
- Cameron, R. H., Duvall, T. L., Schüssler, M., & Schunker, H. 2018, A&A, 609, A56
- Cameron, R. H. & Schüssler, M. 2023, Space Sci. Rev., 219, 60
- Centeno, R. 2012, ApJ, 759, 72
- Charbonneau, P. 2020, Living Reviews in Solar Physics, 17, 4
- Dasi-Espuig, M., Solanki, S. K., Krivova, N. A., Cameron, R., & Peñuela, T. 2010, A&A, 518, A7
- DeVore, C. R., Boris, J. P., & Sheeley, N. R., J. 1984, Sol. Phys., 92, 1
- Gizon, L., Cameron, R. H., Pourabdian, M., et al. 2020, Science, 368, 1469
- Hathaway, D. H. 2011, Sol. Phys., 273, 221
- Hoynig, P. 2003, The field, the mean and the meaning, ed. A. Ferriz-Mas & M. Núñez (London and New York: Taylor & Francis), 1–36
- Kitchatinov, L. L. & Olemskoy, S. V. 2011, Astronomy Letters, 37, 656
- Komm, R. W., Howard, R. F., & Harvey, J. W. 1995, Sol. Phys., 158, 213
- Leighton, R. B. 1964, ApJ, 140, 1547
- Leighton, R. B. 1969, ApJ, 156, 1
- Lemerle, A., Charbonneau, P., & Carignan-Dugas, A. 2015, ApJ, 810, 78
- Linker, J. A., Caplan, R. M., Downs, C., et al. 2017, ApJ, 848, 70
- Mahajan, S. S., Hathaway, D. H., Muñoz-Jaramillo, A., & Martens, P. C. 2021, ApJ, 917, 100
- Muñoz-Jaramillo, A., Nandy, D., & Martens, P. C. H. 2011, ApJ, 727, L23
- Norton, A., Howe, R., Upton, L., & Usoskin, I. 2023, Space Sci. Rev., 219, 64
- Parker, E. N. 1955a, ApJ, 122, 293

- Parker, E. N. 1955b, ApJ, 121, 491
- Schou, J., Antia, H. M., Basu, S., et al. 1998, ApJ, 505, 390
- Sheeley, N. R., Jr., DeVore, C. R., & Boris, J. P. 1985, Sol. Phys., 98, 219
- Steenbeck, M., Krause, F., & Rädler, K. H. 1966, Zeitschrift Naturforschung Teil A, 21, 369
- Unno, W. & Ribes, E. 1976, ApJ, 208, 222
- Waldmeier, M. 1939, Astronomische Mitteilungen der Eidgenössischen Sternwarte Zürich, 14, 470
- Waldmeier, M. 1955, Ergebnisse und Probleme der Sonnenforschung (Leipzig: Akademische Verlagsgesellschaft Geest & Portig)
- Yeates, A. R., Cheung, M. C. M., Jiang, J., Petrovay, K., & Wang, Y.-M. 2023, Space Sci. Rev., 219, 31